PCCP

Accepted Manuscript

ROYAL SOCIETY OF CHEMISTRY

www.rsc.org/pccp

Journal Name

RSCPublishing

ARTICLE

NiO-decorated mesoporous TiO_2 flowers for improved photovoltaic dye sensitized solar cell

Cite this: DOI: 10.1039/xoxxoooooox

Received ooth January 2012,
Accepted ooth January 2012

DOI: 10.1039/xoxxoooooox

www.rsc.org/

Jian Zhi,[a] Angran Chen,[a] Houlei Cui,[a] Yian Xie [a] and Fuqiang Huang [a,b]

Reducing light-induced e-h recombination is important for a dye sensitized solar cell (DSSC), p-type NiO component in TiO_2-NiO nanoparticles was reported to significantly decrease charge recombination, but its photovoltaic efficiency remains below 4% owing to a small surface area. In this work, we used a one-pot self-assembly process to fabricate flower-like mesoporous TiO_2 decorated by NiO oxides, employing a pluronic polymer P123 as a structure directing and pore forming agent. The flower-like porous TiO_2-NiO nanoparticles (F-TiO_2-NiO NPs), possessing a high BET surface of 130 m^2 g^{-1}, are first used as a photoanode in DSSC. These hybrid nanoparticles, decorated with NiO islands, are beneficial for improving photocurrent by increasing dye absorption and suppressing electron-hole recombination. The optimized F-TiO_2-NiO NPs anode (10 μm thick) achieved a power conversion efficiency of 8.20 %, which is 26 % and 47 % higher than pristine flower-like TiO_2 and commercial available P25 anodes, respectively. This efficiency is the highest among the reported TiO_2-NiO hybrid anodes.

Introduction

Dye-sensitized solar cell (DSSC) proposed by O'Regan and Grätzel,[1] has attracted considerable interest.[2-4] Reducing the recombination of light-induced charge carriers in the dye or electrolyte is an effective way to enhance the photovoltaics. Su et al. fabricated layer-by-layer Au nanoparticles onto the working electrode as a Schottky barrier in a water-based DSSC using chemical reduction method. Chou et al. investigated the dye-sensitized solar cells with a layer of TiO_2/Au (or TiO_2/Ag) composite particles as a Schottky barrier.[5] Furthermore, the p-type oxide nanoparticles, such as NiO,[6, 7] $CuAlO_2$,[8] and CuO,[9] were proposed to be as the hole collector and a barrier for charge recombination. The mixture nanoparticle, such as SnO_2/NiO[10] and TiO_2/NiO,[11] were fabricated to promote the performance of the DSSC. Unfortunately, the power conversion efficiencies in these cases are rather low (<4%), owing to their relatively low surface area (below 50 m^2g^{-1}), which results in the insufficient dye absorption.[12]

Another key technology for DSSCs is to design an efficient photoanode with a large specific surface area to adsorb light harvesting molecules.[13] Various titania nano/microstructures, including hollow spheres,[14] forest-like structures,[15] core–shell,[16] shell in shell,[17] and urchin-like nanospheres,[18] were used in fabricating novel photoanodes. Recently, flower-like mesoporous TiO_2 was reported to be composed of nanoscale building blocks,[19, 20] which may be suitable to be employed as an efficient photoanode [21] in DSSCs. The flower-like nanoparticles can effectively enhance light scattering and trapping for efficient photon harvesting and offer a large surface area for dye adsorption, thereby resulting in improved power conversion efficiency.

Herein, we used a self-assembly process to embed island-like NiO oxide particles into flower-like mesoporous TiO_2 through employing a pluronic polymer P123 ($EO_{20}PO_{70}EO_{20}$, Aldrich) as a structure directing and pore forming agent. Small amount (2 mol%) of NiO was decorated into the TiO_2 frameworks, and highly porous flower like TiO_2-NiO nanoparticles (denoted as F-TiO_2-NiO NPs), possessing a high BET surface of 130 m^2g^{-1}, were fabricated after multi-step dip coating, self-assembly and calcination processes. The flower like nanoparticles consist of numerous branched 1D nanorods, which are bundled with each other. Such nanocrystalline structures can not only offer a direct pathway for the rapid collection of photogenerated electrons but also provide a large specific surface area. More importantly, owing to the decoration of NiO, electrons recombination in the dye or electrolyte was also suppressed. Using F-TiO_2-NiO NPs film with a thickness of about 10 μm as anode materials, the DSSCs showed a power conversion efficiency of up to 8.20 %.

Experimental

Materials

Titanium tetraisopropoxide, absolute ethanol, titanium tetrachloride, Nickel(II) nitrate hexahydrate were all of A.R grade and were all purchased from Aladdin Chemical Reagent Co., Ltd, China. Sensitized dye N719 (RuL_2 $(NCS)_2$, L=4,4'-dicarboxylate-2,2'-bipyridine) was purchased from Solaronix SA (Switzerland). P123 ($EO_{20}PO_{70}EO_{20}$) was purchased from Sigma-Aldrich. All reagents were used without further treatment. A fluorine-doped tin oxide conductive glass (FTO glass, with sheet resistance of 8 Ω cm^2, purchased from Hartford Glass Co., USA) was used as a substrate for DSSC test. In order to improve adherence of TiO_2 to FTO surface, the FTO glass was immersed into 0.1 M $TiCl_4$ aqueous solution and followed by sintering process in a furnace at 450 ◦C for 2 h before deposition of anode film. Titania nanopowder (P25) was purchased from Degussa, Germany.

Preparation of F-TiO_2-NiO NPs and F-TiO_2 NPs thin film on FTO glass:

1 g of Pluronic P123 was dissolved in 20 g of ethanol, then 0.6 g of $TiCl_4$ and 2.5 g of titanium isopropoxide were added in that order to the solution and the mixture was further stirred for 2 h. The pH value of the mother solution was *ca.* 1.2. Then 0.07g nickel(II) nitrate hexahydrate(2 mol%) dissolved in 2 ml absolute ethanol was added. After stirring for 2 hours, clear precursor solution was obtained. Single layer of F-TiO_2-NiO NPs thin film on $TiCl_4$ treated FTO glass can be prepared by dip-coating of the precursor solution and gellation at 80 °C for 1 day. The deposition of several layers (with the thickness up to 10 μm) is made by the intercalation of a stabilization step between each coating. This stabilization is performed by heating the fresh film during 15 minutes in an oven pre-heated at 200 °C. Finally, the P123 template was removed after treating the multilayer film at 350 °C under air in a tube furnace with a ramp of 1 °C min^{-1}. The temperature is set at 350 °C for 2 h and the film is allowed to cool down in the oven. The preparation of F-TiO_2 NPs thin film on FTO glass was similar with F-TiO_2-NiO NPs thin film without the addition of nickel(II) nitrate hexahydrate.

Preparation of P25 NPs thin film on FTO glass:

2.5 g of P25 was mixed with 20 ml ethanol, and stirred for 2 hours. The dip coating process of the P25 solution on $TiCl_4$ treated FTO glass was similar with F-TiO_2-NiO NPs thin film. The thickness of P25 NPs thin film was set to 4 um after repeated dip-coating method. Finally, the film was sintered at 350 °C under air in a tube furnace with a ramp of 1 °C min^{-1}, and allowed to cool down to room temperature.

Fabrication of DSSCs:

The obtained TiO_2 thin film deposited on FTO glass was immersed in a 0.05 M $TiCl_4$ aqueous solution at 70 °C for 30 min to improve the photocurrent and photovoltaic performances. After sintering at 450 °C for 30 min, the film was sensitized by a 2.5×10^{-4} M N719 absolute ethanol solution for 24 h to adsorb the dye adequately; thus, a dye sensitized TiO_2 film electrode was obtained. Then, the electrode was sandwiched together with a platinized FTO counter electrode. The redox electrolyte was injected into the aperture between the dye sensitized TiO_2 film electrode and the counter electrode.

Measurements and characterization:

XRD measurements were carried out using powder X-ray diffraction (Bruker D8 Advance, with Cu_KR radiation operating at 40 kV and 40 mA, scanning from 2θ = 20 to 80°). Field emission scanning electron microscopy (FESEM; Hitachi S-4800) and transmission electron microscope (JEOL 2100 TEM, 200 kV) equipped with an X-ray energy-dispersive spectrometer (EDS) were used to characterize the morphology, the crystallinity and the chemical composition of the samples. Nitrogen adsorption desorption isotherms for surface area and pore analyses were measured using a Nova 3200e (Quantachrome instruments). UV_vis absorbance spectra were measured by a Shinmadzu 3600 UV_vis Spectrophotometers. X-ray photoelectron spectroscopy (XPS) (VG ESCA 220i-XL) was performed and collected with a Thermo Scientific KAlpha instrument, using an Al Ka X-ray source at 1486.6 eV. The amount of adsorbed dye was measured by desorbing the dye into 20 mM NaOH solution with equal amount of deionized water and ethanol and followed by absorption measurement of the solution.[22] The amount of NaOH solution was recorded, and the absorption value at 515 nm (as a function of wavelength) was used to calculate the number of adsorbed N719 dye molecules according to the Beer–Lambert law, A = εlc, where A is the absorbance of the UV–visible spectra at 515 nm, ε = 14,100/M cm is the molar extinction coefficient of the dye at 515 nm, l is the path length of the light beam, and c is the dye concentration. The current voltage test of DSSCs were performed under one sun condition using a solar light simulator (Oriel, 91160, AM 1.5 globe,100 mW/cm2). The incident-light intensity was calibrated using a radiant power/energy meter (Oriel, 70260) before each experiment. The incident-photonto-current conversion efficiency (IPCE) spectra were measured using a specially designed IPCE system (Newport Co., USA).EIS experiments were performed under illumination provided by solar light simulator(Oriel, 91160, AM 1.5 globe,100 mW/cm^2) while the cell was biased at the V_{oc} induced by the illumination. The open-circuit voltage decay (OCVD) was recorded by turning off the illumination on DSSC in a steady state and monitoring the subsequent decay of V_{oc}. The above measurements were carried out on the CHI660B electrochemical workstation combined with a Xenon light source.

Results and discussion

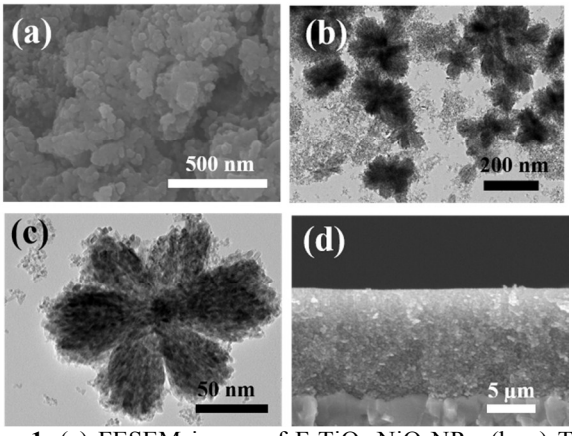

Figure 1. (a) FESEM image of F-TiO_2-NiO NPs. (b, c) TEM images of F-TiO_2-NiO NPs with different magnification. (d) Cross-sectional FESEM image of F-TiO_2-NiO NPs.

The morphology of the F-TiO_2-NiO NPs film was investigated by field emission scanning electron microscopy (FESEM), as shown in Figure 1a. From this image, owing to the small pore size of the nanoparticles, the pore structures are indeed not clearly shown. However, the image clearly shows numerous interconnected grains, which can facilitate rapid electron transport within the TiO_2 film and highly efficient charge transfer at interfaces of film/dye/electrolyte.[23]

Figure 1b clearly shows the overall flower like morphology of F-TiO_2-NiO NPs by TEM characterization. The average diameter of the nanoparticles is about 100-140 nm. Figure 1c is the magnification TEM image of F-TiO_2-NiO NPs. It can be seen that a single F-TiO_2-NiO NPs is composed of needle like nanorods radiating from the center of the sphere. This result occurs because the hydrophilic P123 chains interacting with the water core in the solution are directly hydrolyzed to produce TiO_2 nuclei, which then grow to generate needle-like nanorods from the center of the spheres. The HRTEM image (Figure S2) of F-TiO_2-NiO NPs shows the lattice fringes with a spacing of ca. 0.15 and 0.25 nm, corresponding to the (2 2 0) plane of the face-centered NiO and (112) plane of anatase TiO_2, repectively.[24, 25] From the cross-sectional cut (Figure 1d) it is apparent that our F-TiO_2-NiO NPs photoanodes are sponge-like, in which the channels for electron and ion transport have been well constructed. It is noteworthy that due to the relatively small size (about 100 nm diameter) of F-TiO_2-NiO NPs, the flower shape cannot be found clearly in this large scale morphology.

Elemental mapping by energy-dispersive X-ray spectroscopy (EDS) unambiguously confirmed the island-like structure of the NiO inside TiO_2 NPs, as shown in Figure 2. Uniform distribution of NiO components were observed inside the TiO_2 NPs, indicating the successful introduction of NiO into the framework of flower like TiO_2 NPs. To demonstrate the beneficial barrier effect of NiO components and mesoporous structure of F-TiO_2-NiO NPs, pristine F-TiO_2 NPs and P25 photoanode film were also fabricated through the same method, and the corresponding TEM images were shown in Figure S1 and S2. Without the introduction of NiO, TiO_2 NPs exhibited the similar flower like structure as F-TiO_2-NiO NPs, demonstrating that the decorating of NiO did not affect the formation of TiO_2 NPs (Figure 2). In the case of P25, the particle size is about 25 nm, which is much smaller than TiO_2 NPs (Figure S3).

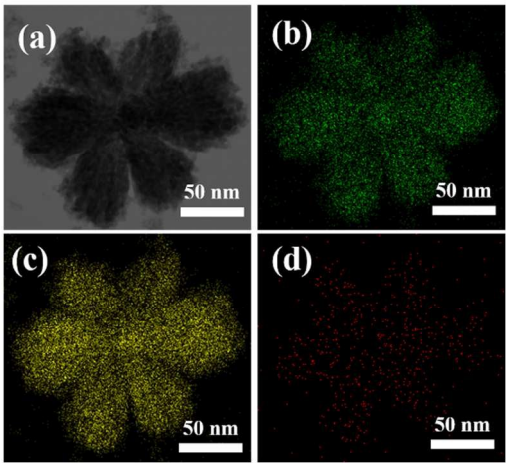

Figure 2. Scanning TEM images of F-TiO2-NiO NPs(a) and the corresponding elemental mapping images of (b) Ti, (c) O and (d) Ni.

The chemical composition of F-TiO_2-NiO NPs was further studied by X-ray photoelectron spectroscopy (XPS) analysis, and the corresponding results are shown in Figure 3. As observed in Figure 3a, the fully scanned spectrum indicates that Ni, Ti, O, and C existed in the F-TiO_2-NiO NPs. The C element could be attributed to the adventitious carbon-based contaminant. Therefore, it was concluded that F-TiO_2-NiO NPs were composed of three elements, Ti, Ni, and O, which is in good agreement with the above EDX results. Figure 3b shows the high-resolution XPS spectrum of the Ni 2p region. According to the previous results, the Ni 2p signal can be fitted into four peaks. The binding energies at 856.8 and 862.9 eV are attributed to the Ni 2p3/2 peaks, and the 874.2 and 880.9 eV peaks are attributed to Ni 2p1/2 within experimental error. The Ni 2p3/2 peaks are assigned to +2 Ni in the NiO/TiO_2 sample, which is consistent with the results of the XRD analysis. [26] The X-ray diffraction pattern of F- iO_2-NiO NPs was also shown in Figure S4. From JCPDS 21-1272, the X ray diffraction patterns of TiO_2 particles comprise peaks of anatase (<1 0 1>, <0 0 4>, <2 0 0>, <2 1 1>, <2 0 4>, <2 2 0> and <2 1 5>). Besides the peaks of anatase TiO_2, the X-ray diffraction patterns of TiO_2-NiO composite particles show that three peaks of nickel oxide at 2θ = 36.8°, 43.6° and 62.9° correspond to the diffraction from the <111>, <200>, and <220> planes, respectively (bunsenite, JCPDS 47-1049). This result clearly demonstrates that NiO components were successfully formed after the process of calcination. The particle size of NiO was about 8.9 nm, calculated from the Sherrer equation.

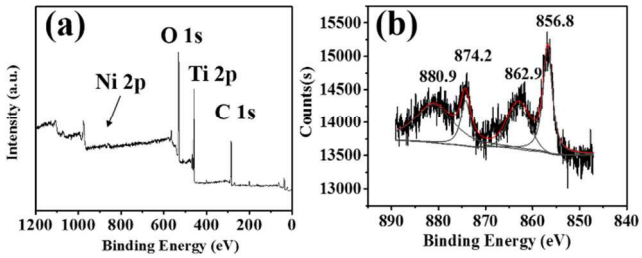

Figure 3. XPS spectra of F-TiO_2-NiO NPs: (a) XPS full spectrum, (b) Ni 2P spectra.

Furthermore, nitrogen adsorption–desorption measurements were conducted to characterize the porous structure of the photoanode. The N_2 adsorption–desorption isotherms of F-TiO_2-NiO NPs, F-TiO_2 NPs and P25 NPs are shown in Figure 4a. Typically, both TiO_2-NiO and F-TiO_2 NPs display the type IV curve ascribed to the predominance of mesopores, while P25 NPs exhibit indistinct porous structure. The Barrett-Joyner-Halenda (BJH) pore size distribution of F-TiO_2-NiO NPs and F-TiO_2 NPs (Figure 4b) indicates a size ranging from 1 to 20 nm, and a peak size of about 10 nm. Moreover, the BET (Brunauer-Emmett-Teller) surface areas of F-TiO_2-NiO NPs and F-TiO_2 NPs are 130 m^2 g^{-1} and 117 m^2 g^{-1}, respectively, much higher than P25 NPs (48 m^2 g^{-1}) and other TiO_2-NiO hybrid particles.[10, 11] A little higher surface area of F-TiO_2-NiO NPs than F-TiO_2 NPs is probably owing to the existence of NiO oxides inside the TiO_2 framework, which may form the tiny cavities between the two kinds of particles. As a result, the dye adsorption capacity of F-TiO_2-NiO NPs and F-TiO_2 NPs is obviously higher than that of P25 NPs.

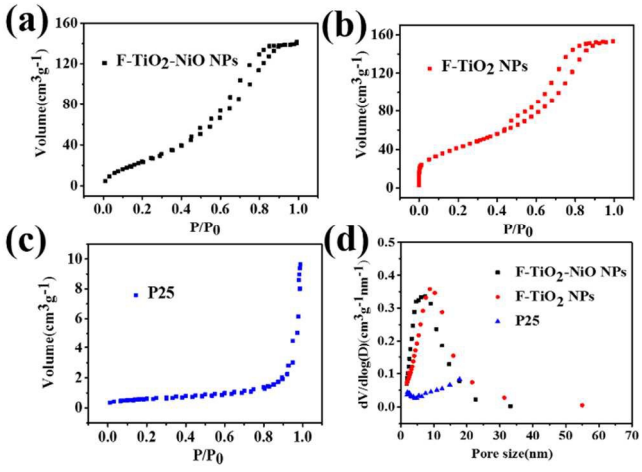

Figure 4. (a-c) Nitrogen adsorption–desorption isotherms of F-TiO_2-NiO NPs, F-TiO_2 NPs and P25 NPs, respectively.(d) BJH pore size distribution curves of F-TiO_2-NiO NPs, F-TiO_2 NPs and P25 NPs

In order to illustrate the light scattering capability of F-TiO_2-NiO NPs, F-TiO_2 NPs and P25 NPs, a comparison of UV-vis spectra of these three different photoanodes is shown in Figure 5a. The absorbance of the flower-like photoanode (F- TiO_2-NiO NPs and F-TiO_2 NPs) is evidently larger than the nanoparticle-based counterpart in visible light region, which may be primarily due to the enhanced light scattering resulting from their highly porous flower like nanostructure with large particle size.[27] The increased absorption in the region of 400-800 nm can arise from the charge transfer transitions in the p-n composites and Ni(II) d-d transition.[28-30] To study the photovoltaic performance of the DSSCs based on different photoanodes, the J–V curves are shown in Figure 5b, and the corresponding photovoltaic characteristics are summarized in table S1 (see supporting information). The overall efficiency, η, was evaluated using the equation $\eta = (FF \times J_{sc} \times V_{oc})/P_{in}$, where FF is the fill factor, J_{sc} is the short circuit current density, V_{oc} is the open-circuit voltage, and P_{in} is the incident light power density. The efficiency increased from 5.56 % for P25 NPs to 6.49 % for F-TiO_2 NPs, and further increased to 8.20 % for F-TiO_2-NiO NPs. This can be attributed to the following factors. Firstly, the specific surface areas of F-TiO_2 NPs and F-TiO_2-NiO NPs are much higher than that of P25 NPs, which enhances the adsorption of dye molecules for the two mesoporous photoanodes (the corresponding dye uptake of the three samples are listed in table S1). Secondly, the introduction of NiO into F-TiO_2 NPs leads to the formation barrier layer. According to the CB and VB potentials of TiO_2, NiO and the ground and excited levels of the Ru-dye shown in Figure 6, photogenerated electrons of the dye adsorbed on TiO_2 layer cannot be transferred back to the CB of NiO, because of the higher CB of NiO than TiO_2 (Figure 6). As a result, the NiO could act as a barrier for electron recombination, leading to higher power conversion efficiency of F-TiO_2-NiO NPs than other two samples.[11, 31] Finally, the optical path within the nanoparticles is extended by the improved light scattering originated by flower like nano-structure, which provides the photons with more opportunities to be absorbed by the dye molecules, resulting in a significant increase of light-scattering capability of F-TiO_2-NiO NPs and F-TiO_2 NPs.[32, 33] It is well known that the film thickness also plays an important role in overall efficiency. With the similar experimental conditions, the optimal thickness for such flower-like nanoparticles based film in this study is about 10 μm. If the film thickness was further increased, the efficiency decreased dramatically, probably owing to the collapse of the bottom layer after multi-step dip-coating process. The thickness of P25 film was also kept in 10 um, which is the most optimized conditions of P25 based photoanode for DSSC.[34]

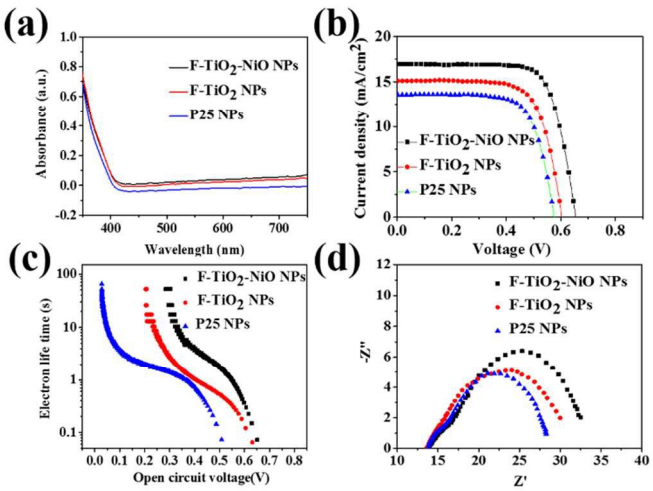

Figure 5. (a) UV-vis diffuse reflectance spectra of F-TiO_2-NiO NPs, F-TiO_2 NPs and P25 NPs, respectively. (b) Photocurrent density-voltage curves. (c) Electron lifetime (in the log-linear representation) as a function of open-circuit voltage (*V*oc). (d) Nyquist plots of the impedance data of the DSSCs with anodes made of F-TiO_2-NiO NPs, F-TiO_2 NPs and P25 NPs.

The open-circuit voltage decay (OCVD) technology has been widely used to study the electron lifetime in a photochemical cell and some other useful information of the recombination process between the injected electrons in TiO_2 and the electrolyte under the open-circuit and dark state.[35-37] The electron lifetime (recombination response time, τ_n) for these devices under open-circuit conditions is calculated from the decay curve of the photovoltage by the following equation 1:

$$\tau_n = -\frac{K_B T}{e}\left(\frac{dV_{oc}}{dt}\right)^{-1}$$

where K_BT is the thermal energy and e is the positive elementary charge. Figure S5 shows the measured OCVD curves of DSSCs with anodes made of F-TiO_2-NiO NPs, F-TiO_2 NPs and P25 NPs. By applying eq.1, the electron lifetime as a function of V_{oc} (V) was plotted in Figure 5c. F-TiO_2-NiO NPs DSSC shows a remarkably increased τ_n over the entire voltage range compared with F-TiO_2 NPs, indicating that the recombination reaction in F-TiO_2-NiO NPs is much slower than F-TiO_2 NPs. When the photogenerated electron transfer in the electrode film, the bare electrode surface area in F-TiO_2 NPs which are not adsorbed by the dyes, can act as a recombination center and the free electron back reaction process will happen through the surface state in this area. After NiO decoration, the back reaction process is restrained owing to the barrier effect of NiO islands, resulting in the enhanced electron life time and cell's performance.[27, 38, 39] Therefore, the open-circuit potential of F-TiO_2-NiO NPs based DSSC (0.66 V) is higher than F-TiO_2 NPs (0.60 V), as shown in table S1. Significantly smaller electron lifetimes in the low voltage region are observed in the P25 NPs compared to the other two anodes, and the corresponding V_{oc} of P25 electrode is 0.57 V. The results also show that the mesoporous TiO_2 based anodes have a lower surface trap density than the P25 anode, as discussed in previously reported literature.[40]

To further explore the kinetics of electrochemical and photoelectrochemical processes, electrochemical impedance spectroscopy (EIS) technique had been employed, as shown in Figure 5d. An equivalent circuit representing the DSSC shown in Figure S6 (ESI†) is adopted to fit the EIS spectra. The electron transport resistance (R_t) and charge-transfer resistance related to

recombination of an electron (R_{rec}) in the three anodes estimated from the impedance analyses are listed in table S1. A larger R_{rec} is obtained in both F-TiO_2-NiO NPs and F-TiO_2 NPs anodes, consistent with the longer lifetimes. The electron diffusion lengths (L_n) in the anodes are further calculated using the relation of $L_n = L\sqrt{R_{rec}/R_t}$, as listed in table S1, where L represents the thickness of photoanode. L_n in both F-TiO_2-NiO NPs and F-TiO_2 NPs anodes is considerably enhanced. Typically, the largest L_n value of F-TiO_2-NiO NPs is attributed to the largest electron lifetime in the anode, originating from the barrier effect of NiO, which is consistent with the results of OCVD analyses.

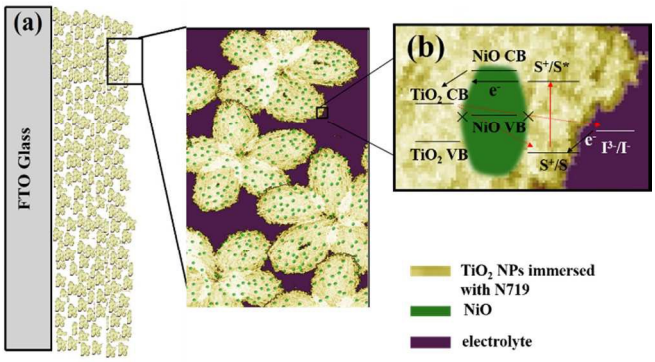

Figure 6. (a) Schematic view of F-TiO_2-NiO NPs anode of DSSC. (b) Illustration of electron transfer inside the composite film.

To elucidate the plausible role of NiO components for improved DSSC properties, a schematic picture of F-TiO_2-NiO NPs was depicted in Figure 6. As shown in Figure 6(b), after the energized electrons transfer to the CB of TiO_2 via tunneling through p-type NiO, the NiO particles can act as a barrier layer for charge recombination between the reduced dye and the electrons in the TiO_2 conduction band.[11] In present work, the NiO particles do not form complete shell around the TiO_2 particles but give an island-like deposit inside the TiO_2 framework. This structure can be considered advantageous in comparison to the previously reported TiO_2-NiO core-shell structure in terms of sensitization and charge injection efficiency.[41] In the latter structure, dye molecules are directly adsorbed onto the deposited shell but not TiO_2. Owing to the higher CB edge of p-type NiO, electron injection into TiO_2 is hindered in agreement to the previous literatures.[42, 43]In contrast, the island-like TiO_2-NiO structure spares some part of TiO_2 surface available for the direct dye adsorption and consequently direct charge injection into TiO_2 CB. As a result, the charge transfer inside the TiO_2 anode is not compromised after the introduction of NiO.[41]

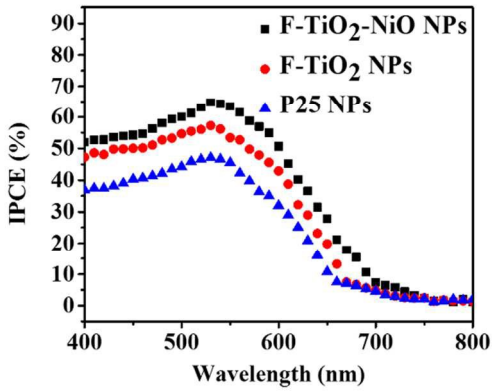

Figure 7. IPCE curves of F-TiO_2-NiO NPs, F-TiO_2 NPs and P25 NPs DSSCs.

The IPCE spectra in Figure 7 offer detailed information in the ability of photo-current conversion of the DSSCs. The IPCE value depends on the light absorption of the dye, the electron injection quantum yield, and the electron collection efficiency. It is observed that the maximum value of the IPCE spectra occurs at around 520 nm. The IPCE of both F-TiO_2-NiO NPs and F-TiO_2 NPs is much higher than that of P25 NPs in the full range, ascribed to the high dye loading and fast electron transport in the mesoporous F-TiO_2 NPs. More importantly, the relatively higher IPCE of F-TiO_2-NiO NPs than that of F-TiO_2 NPs was mainly due to the effectively separating of electron–hole pairs owing to the blocking effect of the NiO particles. As a result, the electrons injected from excited dye can survive longer and hence can facilitate electron transport without undergoing losses at the bare TiO_2 surface.

Conclusions

In summary, the NiO-decorated porous flower-like TiO_2 nanoparticles have been successfully synthesized. The uniformly distributed island-like NiO around TiO_2 constructed a barrier layer inside TiO_2 nanoparticles. Such novel TiO_2-NiO composites improved dye absorption and less e-h recombination, which are beneficial for larger photocurrent. The F-TiO_2-NiO NPs photoanode with a high BET surface of 130 m^2g^{-1} showed a power conversion efficiency of up to 8.20 % in a DSSC, indicating a 26 % and 47 % higher than those of F-TiO_2 NPs and P25-ased DSSCs, respectively. This work finds that F-TiO_2-NiO NPs material has good potential for application in solar cells. The PCE is expected to be further improved by engineering the morphology and thus the surface area and the dye adsorption of the F-TiO_2-NiO NPs.

Acknowledgements

Jian Zhi and Angran Chen contributed equally to this work. This work was financially supported from CAS Project of (Grant no. KGZD-EW-303) and NSF of China (Grant nos. 61376056, 51125006, 91122034, 51121064).

Notes and references

[a]CAS Key Laboratory of Materials for Energy Conversion, Shanghai Institute of Ceramics Chinese Academy of Sciences Shanghai 200050, P. R. China
E-mail: huangfq@mail.sic.ac.cn
[b]Beijing National Laboratory for Molecular Sciences and State Key Laboratory of Rare Earth Materials Chemistry and Applications, College of Chemistry and Molecular Engineering, Peking University Beijing , 100871 , P. R. China

Electronic Supplementary Information (ESI) available: [details of any supplementary information available should be included here]. See DOI: 10.1039/b000000x/

1. B. Oregan and M. Gratzel, *Nature*, 1991, **353**, 737-740.
2. N. S. Lewis, *Science*, 2007, **315**, 798-801.
3. S. Kim, D. Kim, H. Choi, M.-S. Kang, K. Song, S. O. Kang and J. Ko, *Chemical Communications*, 2008, 4951-4953.
4. M. Gratzel, *Journal of Photochemistry and Photobiology a-Chemistry*, 2004, **168**, 235-235.
5. C.-S. Chou, R.-Y. Yang, C.-K. Yeh and Y.-J. Lin, *Powder*

Technology, 2009, **194**, 95-105.
6. J. Bandara and H. Weerasinghe, *Solar Energy Materials and Solar Cells*, 2005, **85**, 385-390.
7. F. Vera, R. Schrebler, E. Munoz, C. Suarez, P. Cury, H. Gomez, R. Cordova, R. E. Marotti and E. A. Dalchiele, *Thin Solid Films*, 2005, **490**, 182-188.
8. J. Bandara and J. P. Yasomanee, *Semiconductor Science and Technology*, 2007, **22**, 20-24.
9. S. Sumikura, S. Mori, S. Shimizu, H. Usami and E. Suzuki, *Journal of Photochemistry and Photobiology a-Chemistry*, 2008, **194**, 143-147.
10. J. Bandara, C. M. Divarathne and S. D. Nanayakkara, *Solar Energy Materials and Solar Cells*, 2004, **81**, 429-437.
11. C.-S. Chou, Y.-J. Lin, R.-Y. Yang and K.-H. Liu, *Advanced Powder Technology*, 2011, **22**, 31-42.
12. G. Shang, J. Wu, M. Huang, Z. Lan, J. Lin, Q. Liu, M. Zheng, J. Huo and L. Liu, *Journal of Materials Chemistry A*, 2013, **1**, 9869-9874.
13. W. Yang, J. Li, Y. Wang, F. Zhu, W. Shi, F. Wan and D. Xu, *Chemical Communications*, 2011, **47**, 1809-1811.
14. H.-J. Koo, Y. J. Kim, Y. H. Lee, W. I. Lee, K. Kim and N.-G. Park, *Advanced Materials*, 2008, **20**, 195-+.
15. F. Shao, J. Sun, L. Gao, S. Yang and J. Luo, *Journal of Materials Chemistry*, 2012, **22**, 6824-6830.
16. J. Du, J. Qi, D. Wang and Z. Tang, *Energy & Environmental Science*, 2012, **5**, 6914-6918.
17. L. Yi, Y. Liu, N. Yang, Z. Tang, H. Zhao, G. Ma, Z. Su and D. Wang, *Energy & Environmental Science*, 2013, **6**, 835-840.
18. J. Lin, A. Nattestad, H. Yu, Y. Bai, L. Wang, S. X. Dou and J. H. Kim, *Journal of Materials Chemistry A*, 2014, **2**, 8902.
19. E. Hosono, S. Fujihara, H. Lmai, I. Honma, I. Masaki and H. Zhou, *Acs Nano*, 2007, **1**, 273-278.
20. A. K. Sinha, S. Jana, S. Pande, S. Sarkar, M. Pradhan, M. Basu, S. Saha, A. Pal and T. Pal, *Crystengcomm*, 2009, **11**, 1210-1212.
21. J.-K. Oh, J.-K. Lee, H.-S. Kim, S.-B. Han and K.-W. Park, *Chemistry of Materials*, 2010, **22**, 1114-1118.
22. W. Q. Wu, Y. F. Xu, H. S. Rao, C. Y. Su and D. B. Kuang, *Nanoscale*, 2013, **5**, 4362-4369.
23. S. R. Gajjela, K. Ananthanarayanan, C. Yap, M. Grätzel and P. Balaya, *Energy & Environmental Science*, 2010, **3**, 838.
24. K.-D. Kim, J. W. Nam, H. O. Seo, Y. D. Kim and D. C. Lim, *The Journal of Physical Chemistry C*, 2011, **115**, 22954-22959.
25. C. Yuan, J. Li, L. Hou, L. Yang, L. Shen and X. Zhang, *Electrochimica Acta*, 2012, **78**, 532-538.
26. B. Zhao, X.-K. Ke, J.-H. Bao, C.-L. Wang, L. Dong, Y.-W. Chen and H.-L. Chen, *Journal of Physical Chemistry C*, 2009, **113**, 14440-14447.
27. K. Fan, W. Zhang, T. Peng, J. Chen and F. Yang, *The Journal of Physical Chemistry C*, 2011, **115**, 17213-17219.
28. C. Shifu, L. Wei, Z. Sujuan and C. Yinghao, *Journal of Sol-Gel Science and Technology*, 2010, **54**, 258-267.
29. W. Wong and M. Malati, *Solar Energy*, 1986, **36**, 163-168.
30. J. Yu, Y. Hai and B. Cheng, *The Journal of Physical Chemistry C*, 2011, **115**, 4953-4958.
31. T. L. Chiang, C. S. Chou, D. H. Wu and C. M. Hsiung, *Advanced Materials Research*, 2011, **239-242**, 1747-1750.
32. L. Feng, J. Jia, Y. Fang, X. Zhou and Y. Lin, *Electrochimica Acta*, 2013, **87**, 629-636.
33. M. Ye, H. Y. Liu, C. Lin and Z. Lin, *Small*, 2013, **9**, 312-321.
34. K. Pan, W. Zhou, G. Tian, Q. Pan, C. Tian, T. Xie, Y. Dong, D. Wang and H. Fu, *European Journal of Inorganic Chemistry*, 2011, **2011**, 4730-4737.
35. H. Yu, S. Zhang, H. Zhao, B. Xue, P. Liu and G. Will, *The Journal of Physical Chemistry C*, 2009, **113**, 16277-16282.
36. M.-H. Kim and Y.-U. Kwon, *The Journal of Physical Chemistry C*, 2011, **115**, 23120-23125.
37. C. C. Yuan, S. M. Wang, W. L. Chen, L. Liu, C. Qin, Z. M. Su and E. B. Wang, *Dalton transactions*, 2014, **43**, 1493-1497.
38. W. Peng, Y. Zeng, H. Gong, Y.-q. Leng, Y.-h. Yan and W. Hu, *Solid-State Electronics*, 2013, **89**, 116-119.
39. A. Zaban, M. Greenshtein and J. Bisquert, *Chemphyschem : a European journal of chemical physics and physical chemistry*, 2003, **4**, 859-864.
40. W.-P. Liao and J.-J. Wu, *Journal of Materials Chemistry*, 2011, **21**, 9255-9262.
41. N. Parsi Benehkohal and G. P. Demopoulos, *Journal of Power Sources*, 2013, **240**, 667-675.
42. A. Kay and M. Grätzel, *Chemistry of Materials*, 2002, **14**, 2930-2935.
43. H. Alarcón, M. Hedlund, E. M. J. Johansson, H. Rensmo, A. Hagfeldt and G. Boschloo, *The Journal of Physical Chemistry C*, 2007, **111**, 13267-13274.